Colloids and Surfaces B: Biointerfaces 210 (2022) 112240

Contents lists available at ScienceDirect

Colloids and Surfaces B: Biointerfaces

journal homepage: www.elsevier.com/locate/colsurfb

Hyaluronan-coated nanoparticles for active tumor targeting: Influence of polysaccharide molecular weight on cell uptake

Francesca Della Sala [a,1], Teresa Silvestri [b,1], Assunta Borzacchiello [a,*], Laura Mayol [c,d,**], Luigi Ambrosio [a], Marco Biondi [b,d]

[a] Istituto per i Polimeri, Compositi e Biomateriali, Consiglio Nazionale delle Ricerche (IPCB-CNR), Viale J.F. Kennedy 54, Napoli, Italy
[b] Dipartimento di Farmacia, Università di Napoli Federico II, Via Domenico Montesano 49, Napoli, Italy
[c] Dipartimento di Scienze Biomediche Avanzate, scuola di Medicina e Chirurgia, Università degli studi di Napoli Federico II, Via Domenico Montesano 49, Napoli, Italy
[d] Centro di Ricerca Interdipartimentale sui Biomateriali (CRIB), Università di Napoli Federico II, Piazzale Tecchio 80, Napoli, Italy

ARTICLE INFO

Keywords:
Hyaluronic acid
Nanoparticle
PLGA
Poloxamer
Cell uptake
CD44 active targeting

ABSTRACT

Here we aimed to correlate different molecular weights of hyaluronic acid (HA), 200, 800 and 1437 kDa, used to decorate poly(lactic-co-glycolic acid) (PLGA)-based nanoparticles (NPs), to their cell uptakes. NP internalization kinetics in CD44-overexpressing breast carcinoma cells were quantified, using healthy fibroblast cells as reference. Actually, NP uptake and selectivity by tumor cells were maximized for NPs HA 800 kDa, while being minimum for NPs HA1400 kDa. This unexpected result could be explained considering that the interaction between NPs and tumor cells is dictated by rearrangement and conformation of that segment of HA chain that actually protrudes from the NPs. Overall, results obtained in this work point at how HA molecular weight, is pivotal project parameter in NP formulation to promote active targeting in the CD44 overexpressing cancer cells.

1. Introduction

Lately, a considerable research focus has been devoted by the scientific community toward the engineering of the surface properties of polymeric nanoparticles (NPs) intended for cancer therapy. In this regard, it is crucial that NPs are bestowed with a sturdy biomimicry demeanour along with the attitude to pointedly target the diseased tissues [1–3]. Indeed, the natural defense mechanisms enclosed in the human body translate into a huge obstacle to the homing of intravenously administered, non-targeted molecules or nanodevices toward the desired biological districts [4]. For example, less than 0.01% of non-targeted drugs do actually reach cancerous lesions after systemic intravenous administration [5].

In this regard, hyaluronic acid (HA) plays a momentous role. Actually, HA is an anionic polysaccharide, composed of repeating units of D-glucuronic acid and N-acetyl-D-glucosamine, belonging to the glycosaminoglycan family [6,7]. HA is a main component of the extracellular matrix (ECM) of mammalia and is involved in manifold mechanical and cell instructive activities [8–10]. More in detail, HA possesses a strong tropism toward solid tumors due to its aptitude for a specialized interplay with CD44 receptors, which are overexpressed on the cytoplasmatic membrane of a wide array of tumour cell populations [11]. In addition, the well-known biocompatibility, biodegradability and non-immunogenicity of HA makes it an extremely attractive material for the surface decoration of nanoplatforms designed to be equipped with active tumour targeting properties [7,12,13].

HA binding to CD44 receptor is affected by multifarious morphological and physico-chemical properties, such as HA molecular weight (MW) [14], spatial arrangement (e.g. cables or pericellular coats) [15,16] or the possibility of receptor cluster induction [17]. Indeed, the mode of ligand presentation is a major determinant of nanocarrier uptake: previous studies have suggested that HA-coated NPs can be internalised following a receptor-mediated pattern [18,19].

In this scenario, the molecular weight of HA can be envisaged as a paramount design parameter in the engineering of nanoplatforms intended for active tumour targeting. Thus, here we aimed to correlate

* Correspondence to: Istituto per i Polimeri, Compositi e Biomateriali, Consiglio Nazionale delle Ricerche (IPCB-CNR), Viale J.F. Kennedy 10 54, Napoli, Italy
** Corresponding author at: Dipartimento di Scienze Biomediche Avanzate, scuola di Medicina e Chirurgia, Università degli studi di Napoli Federico II, Via Domenico Montesano 49, Napoli, Italy
E-mail addresses: bassunta@unina.it (A. Borzacchiello), laumayol@unina.it (L. Mayol).
[1] Equal contribution

https://doi.org/10.1016/j.colsurfb.2021.112240
Received 30 April 2021; Received in revised form 29 October 2021; Accepted 18 November 2021
Available online 24 November 2021

the MW of HA externally exposed and physically linked to poly(lactic-co-glycolic acid) (PLGA)-based NPs to their internalization kinetics in CD44 overexpressing cells. More in detail, three formulations were produced with HA at 200, 800 and 1435 kDa as representative of low, medium, and high molecular weights of the polysaccharide, namely respectively HA2, HA8 and HA14. Prior to NP production, HA concentrations in the external aqueous phase were chosen in order to ensure equal viscosities of the water phase solutions, which was assessed by preliminary rheological experiments. This was crucial because the viscosity of the dispersing phase directly determines the size of the precipitated NPs. Indeed, our aim was to produce NPs with equal size so that differences in cell uptake could be ascribed only to HA MW. The produced NPs were characterized for their technological and thermal properties. NP internalization kinetics were quantified in CD44-overexpressing breast carcinoma cells (HS578T), using healthy mouse fibroblast (L929) cells as a reference. Experimental results were compared with the numerical simulations obtained with a kinetic internalization model based on a cell membrane adsorption-desorption pseudo-stoichiometric balance [20].

2. Material and methods

2.1. Materials

HA with a weight-average MW of 200, 800 and 1435 kDa, were kindly provided by Altergon Italia. Equimolar PLGA (Resomer® RG504H, Mw = 38–54 kDa), Nile red (NR) (9-diethylamino-5-benzo [a] phenoxazinone), fluorescein isothiocyanate (FITC) – phalloidin, 4′,6-diamidino-2-phenylindole (DAPI), along with control L929 cells originating from Mouse C34/An connective tissue from European Collection of cell cultures, were obtained from Sigma-Aldrich (USA). CD44-overexpressing human breast carcinoma cell line (HS578T) were kindly gifted by Dr. Olga Zeni (IREA-CNR). Poloxamer F127 and F68 were from Lutrol (BASF, Ludwigshafen, Germany). Phosphate buffer saline (PBS) tablets without calcium and magnesium were from MP Biomedicals Inc. Penicillin, streptomycin (10,000 U/mL) from Invitrogen and Life Technologies (Carlsbad, CA) were employed. Trypsin and Ethylenediaminetetraacetic acid (EDTA) were from HiMedia (Mumbai, India). Fetal Bovine Serum(FBS) from Lonza (Basel, Switzerland) and Bovine insulin from Gibco EfficientFeed + Supplements (ThermoFisher Scientific, USA) were used.

2.2. Rheological tests

Cell uptake of NPs is dramatically affected by NP size. Therefore, NP production conditions were set to ensure equal NP diameters irrespective of HA MW. This prerequisite could be met by ensuring that the aqueous phase used to prepare NPs (see Section 2.3) possess the same viscosity at a shear rate comparable to the magnetic stirring rate used to fabricate the NPs (approximately 500–600 rpm). To this aim, preliminary rheological tests were performed using a MARS rheometer™ III, HAAKE™ (TermoFisher Scientific, USA). Specifically, oscillatory shear tests were carried out at room temperature, in the linear viscoelasticity region of the samples, in the 5–50 Hz frequency range.

2.3. Nanoparticle preparation

NPs were prepared using nanoprecipitation technique [21,22], followed by solvent evaporation. Briefly, 5 mL of an organic phase (O), composed of a solution of PLGA, F68 and F127 (PLGA:F68:F127 weight ratio was fixed at 1:0.5:0.5) in acetone, were forced through a syringe needle (22 G) at a 333.3 μL/min flow rate by a syringe pump. The solution was precipitated in 40 mL of an aqueous phase, containing F127 and F68 as surfactants (1:1 wt ratio; 5 mg/mL overall concentration) and different amounts of HA. More specifically, HA concentrations were set at 3.75, 0.75 and 0.5 mg/mL for HA2, HA8 and HA14, respectively. For cellular uptake experiments, 10 μL of a fluorescent NR solution were added in acetone. Theoretical dye concentration was 0.01% w/w with respect to the mass of polymer powders. Acetone was evaporated by mechanical agitation for 4 h, and the resulting suspension was washed three times by centrifugation to eliminate the non-encapsulated NR (10, 000 rpm, 10 min).

2.4. Nanoparticle morphology, mean size, size distribution, yield and ζ potential

NP morphology was investigated by transmission electron microscopy (TEM, FEI Tecnai G12 Spirit Twin) with emission source LaB6 (120 kV, spotsize 1) using 400 mesh carbon-coated copper grids at room temperature (RT). The carbon-coated copper grid was immersed in ultradiluted NP suspensions and, after the drying phase, the grid was placed on a rod holder for the TEM characterization. Three grids *per* NP suspension were prepared and a minimum of four micrographs *per* grid were acquired. Intensity-average diameters and ζ potentials of NPs were determined via dynamic light scattering (DLS) measurements with a Zetasizer Nano (Malvern Instruments, Malvern, UK). For particle size measurements, NPs were suspended in ultrapure water. NP yield describes the percentage of recovered NPs expressed as weight of recovered NPs after production with respect to the initial mass of employed materials. It was gravimetrically calculated after lyophilization for 24 h (HetoPowerDry PL6000 Freeze Dryer, Thermo Electron Corp., USA; −60 °C, 0.73 hPa), on the overall recovered mass of NPs. Results were averaged on at least five measurements.

2.5. Nanoparticle stability study

The stability of NP formulations in suspension was assessed by monitoring the trend of the size and polydispersity index in different storage (4 °C, 25 °C, 37 °C) conditions in PBS at pH= 7.4 for 10 days. The NP stability was also evaluated in the conditions of in vitro cellular uptake experiments by suspending NPs in DMEM (cell culture medium supplemented with 10% fetal bovine serum and antibiotics, penicillin G sodium 100 U/mL, streptomycin 100 ug/mL, at 37 °C and 5% CO_2 37 °C for 72 h). NP suspensions were tested by DLS. The results are expressed as average values obtained from three independent measurements.

2.6. Thermal analyses

Thermoanalytical tests were carried out on PLGA, HA and poloxamer powders, along with freeze-dried HA2, HA8 and HA14 NPs, to study the interactions between the different polymers in NP formulations, using a differential scanning calorimeter (DSC; DSC Q20, TA Instruments, U.S.A.) calibrated with a pure indium standard. The samples were placed in aluminum pans and underwent a double scan from −60–80 °C at 5 °C/min. The first scan was carried out to eliminate the thermal history of the samples. All measurements were run under an inert nitrogen atmosphere, purged at a flow rate of 50.0 mL/min. The heat evolved during DSC thermal events (W/g) was calculated from DSC thermograms by integrating the exothermic/endothermic peaks, while the glass transition temperature (T_g) was obtained from thermogram inflection point.

2.7. Cell culture

Breast carcinoma HS578T cells were chosen as a model of cells naturally overexpressing CD44 receptor, while normal L929 cells (passage 15–23) were used as a control, since they have a low degree of CD44 expression [21]. Cells were grown in T-75 cell culture flask (Falcon, Italy), in DMEM cell culture medium supplemented with 10% fetal bovine serum and antibiotics (penicillin G sodium 100 U/mL, streptomycin 100 ug/mL) at 37 °C and 5% CO_2. The medium used for HS578T cells was also enriched with 10 μL/mL bovine insulin. When confluent growth was reached, the cells were detached with 0.25% trypsin - EDTA

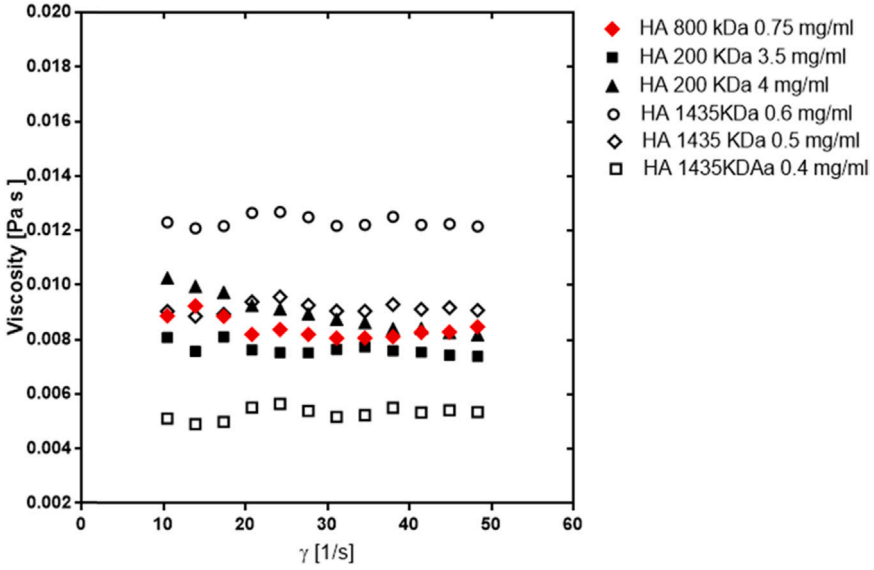

Fig. 1. Flow curves of aqueous solutions of HA at 800 (red), 200 (black) and HA 1435 kDa (white) at different concentrations.

solution and washed twice with PBS. The resulting cell suspensions were centrifuged (5 min, 1000 rpm; BRK55/10 Centrifuge by Centurion Scientific Ltd, UK), the supernatant separated, and the cells re-suspended in fresh culture medium. Viable cells were counted using the TC20 automated Cell Counter (Biorad, USA).

2.8. Confocal microscopy for NP uptake in L929 and HS578T cells

For confocal microscopy acquisitions, 2×10^4 cells were seeded in 1 mL of medium on 35 mm-diameter Fluoro dish cell culture dish (World Precision Instruments, Inc). Cells were incubated for 24 h at 37 °C in a 5% CO_2 atmosphere with a suspension of NPs in the cell culture medium (1 mg/mL for the three formulations). After 24 h, non-internalized NPs were removed by washing twice the samples with PBS, fixed with 10% formalin (Sigma-Aldrich) for 1 h and permeabilized with 0.1% Triton X-100for 3–5 min. Actin filaments were stained with FITC-phalloidin in PBS for 30 min at 25 °C. After two washes with PBS to remove unbound phalloidin conjugate, cell nuclei were stained with DAPI for 10 min at 37 °C. Samples were observed by a confocal microscope (Leica TCS SP8) using a 63X oil immersion objective. Images acquired with a resolution of 1024 × 1024 pixel.

2.9. Quantification of NP uptakes in L929 and HS578T cells

To quantify NPs cell internalization, 2×10^4 L929 or HS578T cells were seeded in 1 mL of cell culture medium in 24 wells. Cells were incubated in the presence of NP suspensions (1 mg/mL) in cell culture medium for 1,3,6,24,48 and 72 h. Subsequently, cells were rinsed twice with PBS and lysed with 0.1 mL of lysis buffer [23]. Cell lysates were then diluted with 0.4 mL of PBS and analyzed by spectrofluorimetry (Multilabel Counter, 1420 Victor, Perkin Elmer), at a 525–605 nm wavelength. Fluorescence intensity of experimental points was interpolated with the calibration curve obtained using known concentration of fluorescent NPs for each formulation (0–0.5 mg/mL). The concentration of internalized NPs was normalized to the number of seeded cells to obtain the number of internalized NP *per* cell taking into account the average NP diameter.

2.10. NP uptake kinetics

Numerical simulations of NP uptake were run by using a single cell model. NP interactions with cells has been schematized as a process consisting of two steps in series, namely NP binding on cell membrane, followed by either NP internalization or desorption. Assuming system homogeneity, cell uptake was described by a second-order pseudo-chemical equilibrium equation [20,24], describing the stoichiometric exchange between NPs and cell membrane, as depicted in the following:

$$NP + \text{cell surface} \longleftrightarrow^{k_B,k_D} NP - \text{cell surface} \longrightarrow^{k_i} NP \text{ internalization} \quad (1)$$

In Eq. (1), k_B [h^{-1}], k_D [mg • mL^{-1} • h^{-1}] and k_i [h^{-1}] are the kinetic coefficients of NP binding, de-binding and internalization. NP uptake has been hypothesized to occur on the *reactive surface* [25–27], i.e. the fraction of cell surface involved in internalization, that is considered to be instantly restored after each uptake event. Cell uptake capacity has been hypothesized to be superiorly limited and, consequently, a maximum number of NPs that can be internalized (N_{MAX}), characteristic for each cell population, has been defined.

Letting N_B be the number of NPs bound to cell surface at time t, C_{NP}^{medium} the time-dependent NP concentration within the cell culture medium and N_i the number of internalized NPs, the time trend of N_B can be expressed by the ensuing mass balance:

$$\frac{dN_B}{dt} = k_B C_{NP}^{\text{medium}}(N_{MAX} - N_B) - k_D N_B - \frac{dN_i}{dt} \quad (2)$$

Besides, the rate of NP internalization is reasonably surmised to be proportional to the number of bound NPs, i.e.:

$$\frac{dN_i}{dt} = k_i N_B \quad (3)$$

Lastly, the total number of NPs is given by:

$$N_T = N_B + N_i \quad (4)$$

Given the experimental conditions, C_{NP}^{medium} is a major driving force of internalization process, which has been modelled keeping in mind that the rate of NP consumption within the culture medium equilibrates the rate of NP adsorption and internalization (i.e., N_T). Letting n_{cells} denote the number of cultured cells, V_{medium} the cell culture medium volume and ρ_{NP} NP density, it is:

$$\frac{dC_{NP}^{\text{medium}}}{dt} = -\frac{\pi d^3}{6} n_{\text{cells}} V_{\text{medium}} \rho_{NP} \left(\frac{dN_B}{dt} + \frac{dN_i}{dt}\right) \quad (5)$$

The set of ordinary differential Eqs. (1–4) has been fit to the experimental results, with k_B, k_D, k_i and N_{MAX} as adjustable parameters.

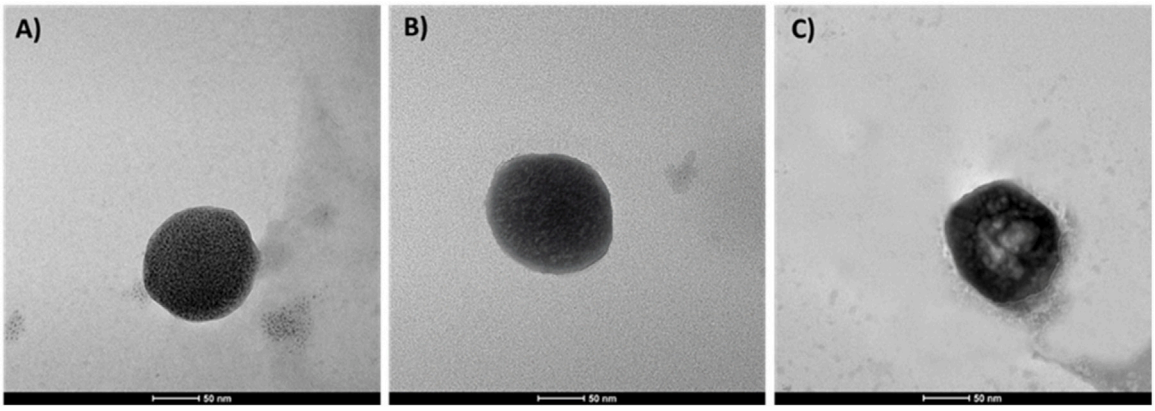

Fig. 2. Selected TEM micrographs of HA2 (A), HA8 (B) and HA14 (C).

Table 1
(A) Main technological features of the produced NPs. (B) Size, Polydispersity Index values of HA2, HA8,HA14 at 4, 25, 37 °C in PBS pH= 7.4. (C) Time evolution of NPs diameter and Polydispersity Index in cell culture medium.

A)	d [nm]	PDI	ζ-potential [mV]	Yield [%]			
HA2	141 ± 3	0.167 ± 0.010	-46.8 ± 1.2	50 ± 15			
HA8	131 ± 7	0.054 ± 0.004	-44.7 ± 1.3	53 ± 10			
HA14	145 ± 15	0.052 ± 0.006	-46.3 ± 1.3	43 ± 34			
B)		HA2		HA8		HA14	
T [°C]	t [day]	d [nm]	PDI	d [nm]	PDI	d [nm]	PDI
4	0	133 ± 3.0	0.087 ± 0.03	122 ± 0.30	0.16 ± 0.08	131 ± 1.4	0.06 ± 0.02
	3	127 ± 0.3	0.056 ± 0.02	133 ± 3.2	0.14 ± 0.01	127 ± 0.3	0.056 ± 0.02
	7	129 ± 2.0	0.09 ± 0.04	126 ± 0.3	0.05 ± 0.04	129 ± 2.0	0.09 ± 0.04
	10	129 ± 0.5	0.06 ± 0.02	128 ± 2.0	0.08 ± 0.003	129 ± 0.5	0.06 ± 0.02
25	0	133 ± 3.0	0.087 ± 0.03	122 ± 0.30	0.16 ± 0.08	131 ± 1.4	0.06 ± 0.02
	3	123 ± 1.0	0.085 ± 0.01	125 ± 2.3	0.09 ± 0.02	135 ± 2.3	0.06 ± 0.03
	7	125 ± 2.0	0.05 ± 0.02	133 ± 5.4	0.12 ± 0.06	136 ± 1.3	0.05 ± 0.01
	10	126 ± 0.05	0.09 ± 0.02	124 ± 0.3	0.08 ± 0.01	135 ± 2.2	0.07 ± 0.01
37	0	133 ± 3.0	0.087 ± 0.03	122 ± 0.30	0.16 ± 0.08	131 ± 1.4	0.06 ± 0.02
	3	126 ± 11	0.060 ± 0.08	124 ± 0.93	0.05 ± 0.02	134 ± 1.0	0.04 ± 0.35
	7	129 ± 3.3	0.06 ± 0,03	122 ± 2.0	0.07 ± 0.01	131 ± 1.1	0.10 ± 0.04
	10	122 ± 1.2	0.08 ± 0.03	118 ± 1.4	0.07 ± 0.01	128 ± 1.0	0.08 ± 0.02
C) Formulation	t [day]	d [nm] [± SD]	PDI [± SD]				
HA2	0	133 ± 3.0	0.087 ± 0.03				
	1	134 ± 2.0	0.20 ± 0.02				
	2	129 ± 2.0	0.20 ± 0.01				
	3	126 ± 3.0	0.20 ± 0.03				
HA8	0	122 ± 0.30	0.16 ± 0.08				
	1	124 ± 2.1	0.20 ± 0.01				
	2	115 ± 3.0	0.20 ± 0.02				
	3	117 ± 6.0	0.32 ± 0.03				
HA14	0	131 ± 1.4	0.06 ± 0.02				
	1	135 ± 1.0	0.20 ± 0.03				
	2	133 ± 2.3	0.20 ± 0.03				
	3	145 ± 1.1	0.30 ± 0.03				

2.11. Statistical analysis

Results are reported as the mean of at least three replicas ± standard deviation (SD). Statistical analyses were performed using a one-way analysis of variance (ANOVA) and p values < 0.05 were considered statistically significant.

3. Results and discussion

3.1. Rheological tests

The main objective of this work was to evaluate how the MW of HA decorating the surface of NPs influences cell internalization selectivity and kinetics. Since cell internalization kinetics strongly depend upon NP dimension and superficial properties, preformulation conditions were tailored to ensure that NPs of comparable size could be obtained regardless of the formulation variable. More in detail, during nanoprecipitation, NP size is primarily dependent on the viscosity of the external aqueous phase. Consequently, preliminary rheological tests were performed on the external aqueous phase to determine the concentration of HA that guarantees the same viscosity for the external phases containing HA at the three different MWs. Fig. 1 shows the flow curves, i.e., the dependence of viscosity upon the shear rate of the solutions analysed.

In the analysed frequency range, the viscosity of the solutions was almost constant, exhibiting the pseudo-Newtonian plateau, which is due to a progressive alignment of HA macromolecules. Results showed that similar viscosities were obtained with very different HA concentrations. More in detail, the concentrations of the aqueous phase were set at 3.75, 0.75 and 0.5 mg/mL for HA 200, 800 and 1435 kDa, respectively, corresponding to molar HA concentrations in the external aqueous phase in the range of $0.7 \div 3.0 \cdot 10^{-8}$ mol/L. These conditions allowed the obtainment of NPs with comparable sizes (see below) and can be reasonably associated to a HA density on NPs of comparable order of

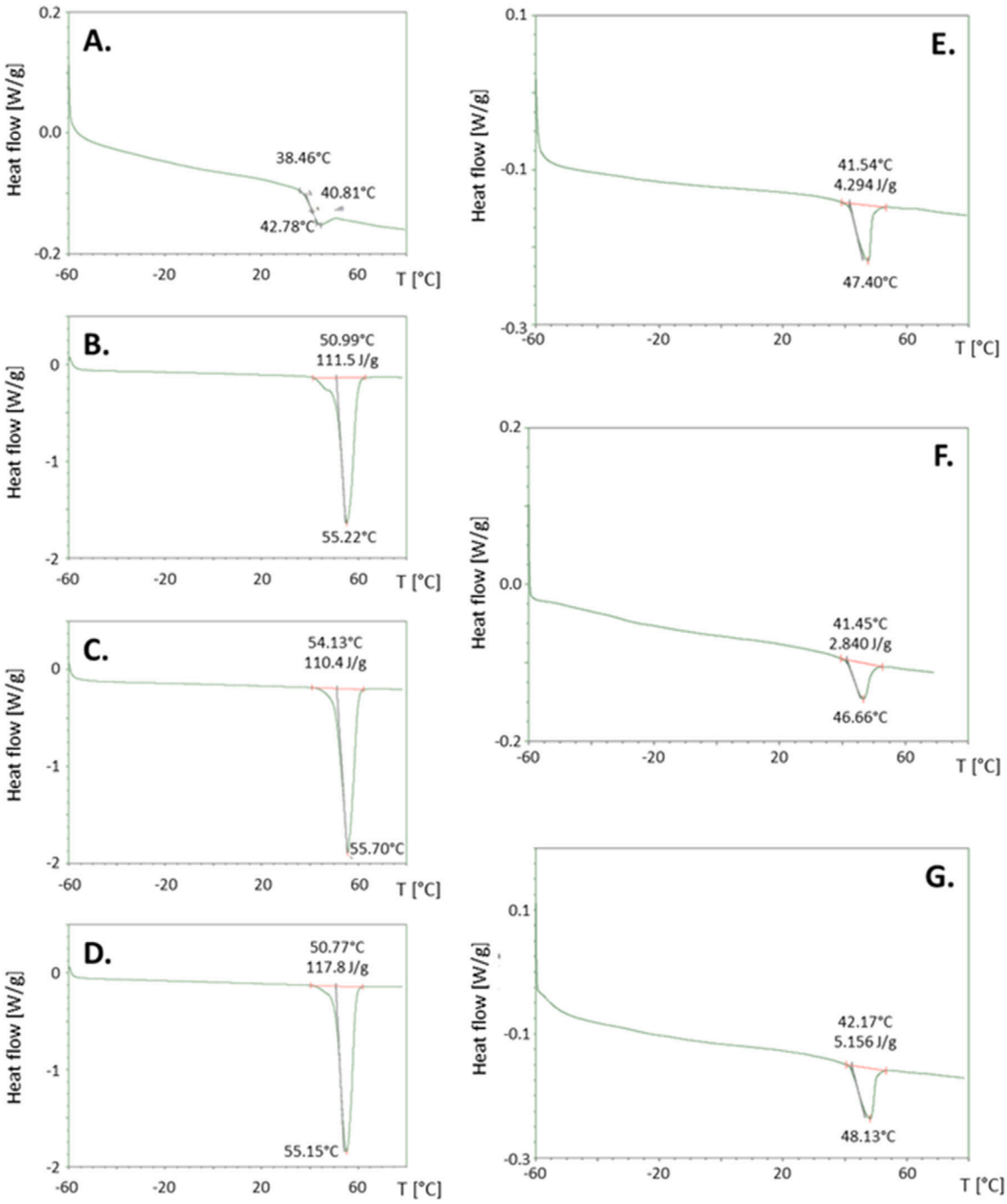

Fig. 3. Representative DSC thermograms of raw PLGA (A); raw F68 (B); raw F127 (C); F68/F127 50/50 w/w physical mixture (D); HA2 NPs (E); HA8 NPs (F); HA14 NPs (G). Exotherm is directed upward.

magnitude.

3.2. Nanoparticle characterization and stability

In order to study the morphology of the three NP formulations, TEM images have been acquired. Selected micrographs of NPs (Fig. 2A, B and C) revealed discrete, spherical particles for all NP formulations.

Mean size, polydispersity index (PDI), yield and ζ potential of the obtained NPs are summarized in Table 1A. Uniform NP sizes and narrow size distributions were found out; mean diameter values were < 150 nm, which are appropriate for intravenous NP administration. These outcomes show that HA concentrations used in the dispersing phase are suitable for a proper control over NP size. Moreover, zeta potentials were similar for HA2, HA8 and HA14 NPs, indicating that charge densities are comparable on the three different formulations. This, in turn, suggests that the number of monomeric units of HA exhibited on the surface of the different NP formulations are similar.

The results obtained confirm the NP stability in each different storage (4, 25, 37 °C) and medium (PBS and DMEM) conditions. Indeed, as shown in Table 1B and C, the mean diameter and the polydispersity index are comparable throughout the duration of study. The same trend was also observed also in vitro cellular uptake experiments conditions.

Table 2
Glass transition/melting temperatures and melting heats of polymers and NPs.

	Tg [°C]	Tonset [°C]	Tpeak [°C]	ΔHm [J/g]
PLGA	41.2 ± 0.7	–	–	–
F68	–	50.9 ± 0.1	54.9 ± 0.5	121 ± 14
F127	–	51.9 ± 1.1	56.0 ± 0.5	116 ± 1
F68 + F127 mixture		51.0 ± 1.3	55.2 ± 0.2	121 ± 5
HA2		42.0 ± 0.7	48.3 ± 1.4	4.13 ± 0.24
HA8		41.5 ± 0.1	46.1 ± 0.8	2.71 ± 0.18
HA14		42.2 ± 0.4	48.3 ± 0.5	4.88 ± 0.25

3.3. Thermal analyses

DSC traces of HA (first and second scan) showed no thermodynamic event in all cases (data not shown), while the thermograms of poloxamers (first scan; Fig. 3B, C, D) showed endothermic peaks, associated to the melting temperature (Tm), at 54.9, 56.0 and 55.2 °C for F68 and F127 and their 50:50 w/w mixture, respectively. Endothermic peaks attributable to poloxamers were also identified in all the first scan of NP formulations, but at lower temperatures (46.1 ÷ 48.3 °C), indicating a plasticizing effect of PLGA and HA toward poloxamers (Fig. 3E, F, G). Furthermore, the heat generated during poloxamers melting (ΔHm) was drastically lower than ΔHm of the raw materials. This bespeaks the loss of most of poloxamers crystalline regions within the rubbery phase of PLGA, which is completely amorphous. Thus, these data clearly indicate that PLGA and poloxamers are mixed at the molecular level, with an only modest phase separation, thereby forming a mainly co-amorphous system within NPs. Moreover, no thermodynamic events were detected in the second DSC scans (data not shown), therefore indicating that the polymeric blend is completely amorphous after the first heating.

Interestingly, HA8 formulation showed the minimal melting heat, while being comparable in the case of HA2 and HA14 formulations. This result points at a preferential interaction between 800 kDa HA with the hydrophilic segments of poloxamers, thereby limiting the formation of crystalline regions of poloxamer macromolecules in NPs. More specifically, considering that the interaction between the hydrophilic poloxamer segments and HA occurs in the external aqueous phase during NP preparation, it is possible to speculate that, in the case of HA2, polysaccharide chain is too short to properly interact with the hydrophilic poloxamer segments. On the contrary, as for HA14 NPs, the polysaccharide backbone is long enough to form coils in the water phase rather than intruding within the hydrophilic regions of the poloxamers. Table 2.

3.4. NP cell uptake

Cell uptake experiments were performed on HS578T breast carcinoma cells, which were chosen as a model of CD44-overexpressing cells, as widely reported in literature [28–30], using healthy L929 fibroblasts as a control. The qualitative uptake of HA2, HA8 and HA14 NPs in HS578T and L929 cells was firstly assessed by confocal microscopy, after 24 h of incubation. Representative images for HS578T (Fig. 4A-B-C) and L929 cells(Fig. 4D-E-F), show a more extensive red fluorescence intensity of NPs in tumor cells compared healthy cells. Specifically, NP fluorescence intensity in both cells was homogeneously diffused in the cytoplasm and prevalently in the perinuclear region. Anyhow, the intracellular fluorescence intensity seemed to be lower in L929 cells than in HS578T cells, thereby suggesting a more facile internalization of NPs in this latter case. These outcomes are consistent with the results obtained in previous works [21,22] and can be attributed to both a greater deregulation of the cytoskeletal apparatus of the tumor cells [31] and the well-known upregulation of CD44 receptor.

3.5. Quantification and kinetics of NP uptake in L929 and HS578T cells

NP selectivity towards tumor cells was assessed by quantifying fluorescent NR-loaded NPs after lysing cells membranes at different times of NPs exposure of both tumor and control cells. It must be underlined that NR is solubilized in acetone in the organic phase of the emulsion used to formulate the NPs and the unencapsulated fraction of

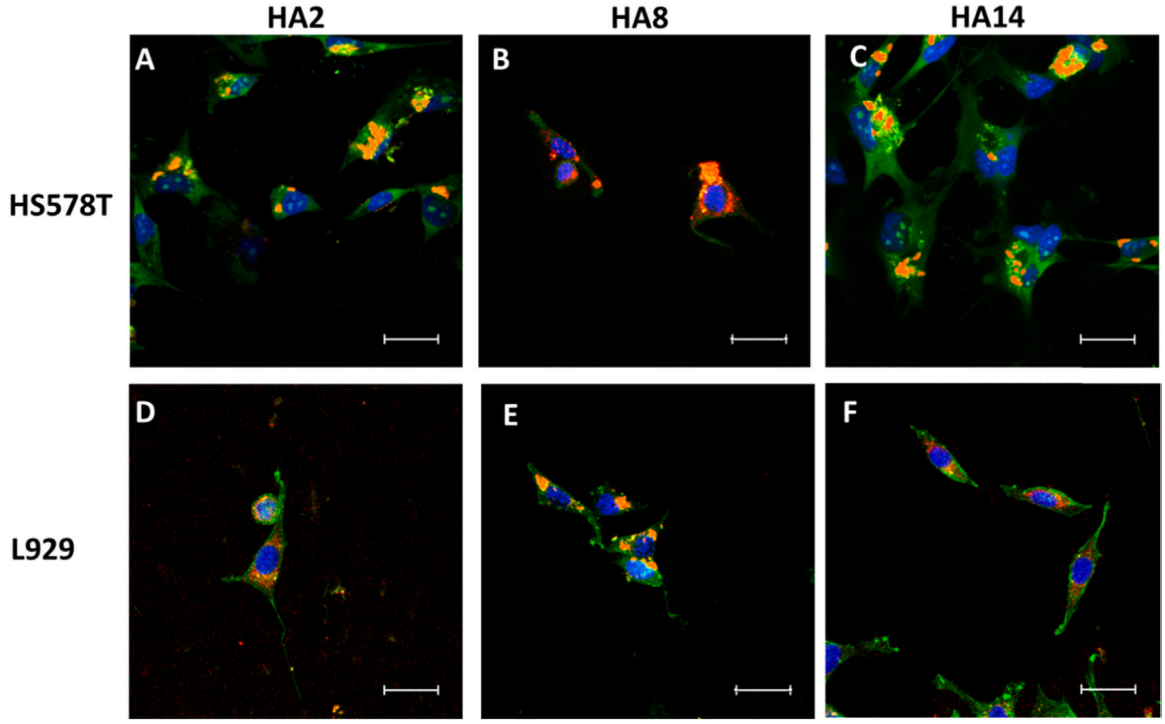

Fig. 4. Confocal images of HS578T and L929 cells exposed to HA2 (A-D) HA8 (B-E) and HA14 (C-F) NPs after 24 h incubation. Maximum projection of Z-stack. Different colours are applied to improve visualization: nuclei (DAPI) are shown in blue; actin filaments (phalloidin) in green; nanoparticles in red. Scale bar: 50 μm. (For interpretation of the references to colour in this figure, the reader is referred to the web version of this article.)

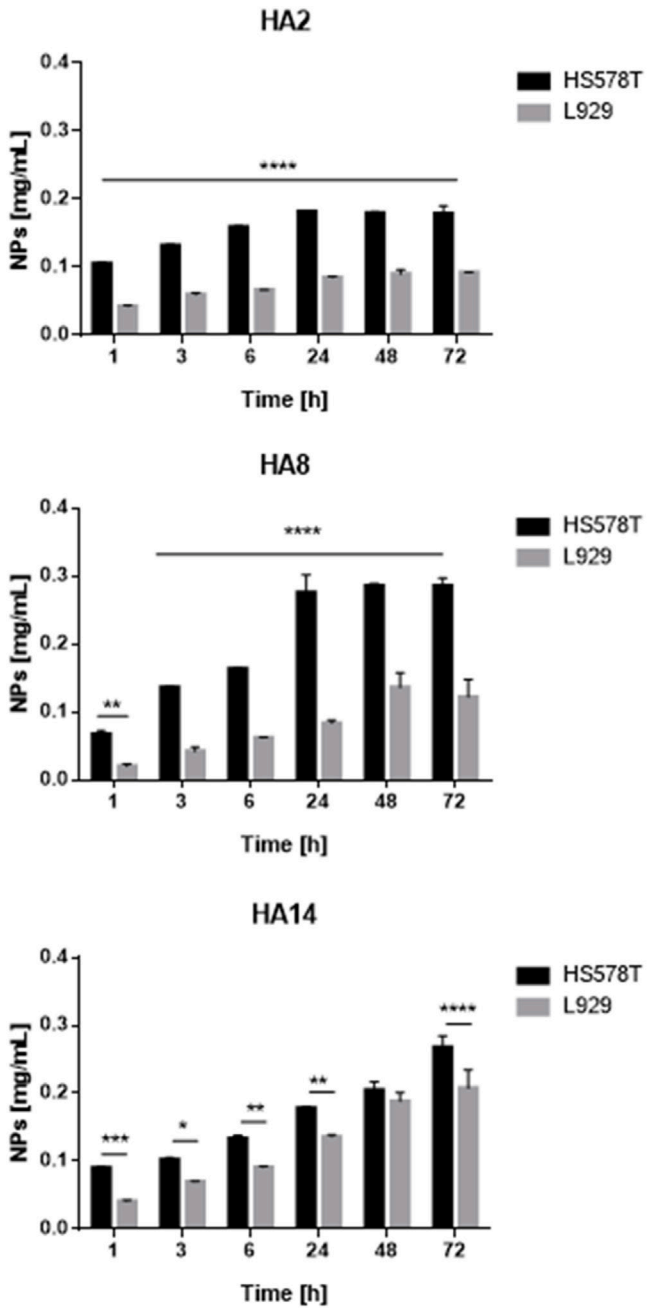

Fig. 5. NP uptakes histograms of HA2, HA8 and HA14, at different exposure time (1, 3, 6, 24, 48 and 72 h), expressed as concentration of NPs [mg/mL] internalized in L929 and HS578T cells.

the dye was eliminated during NP purification and PBS washing.

The results of NP uptake experiments are shown in Fig. 5. In all cases, NP uptake was found to be increasing with exposure time, and a plateau was evidenced after 24 h for HA2 and HA8 formulations, while occurring after about 48 h of incubation for HA14 NPs in L929 cells.

NP uptake results evidenced that the internalization is higher for HS578T than L929 cells in all cases, and this can be easily related to the overexpression of CD44 receptor on HS578T surface and therefore attributed to the promoted tropism for tumor cells induced by the external decoration of NPs with HA. Beyond this evidence, the internalization kinetics are different for the three NP formulations. Indeed, concerning HS578T cells it has been noted that, after 1 h of exposure, similar amounts of HA2 and HA14 NPs were internalized, while a lower uptake was detected for HA8 NPs. After 6 h exposure, the uptake of HA2

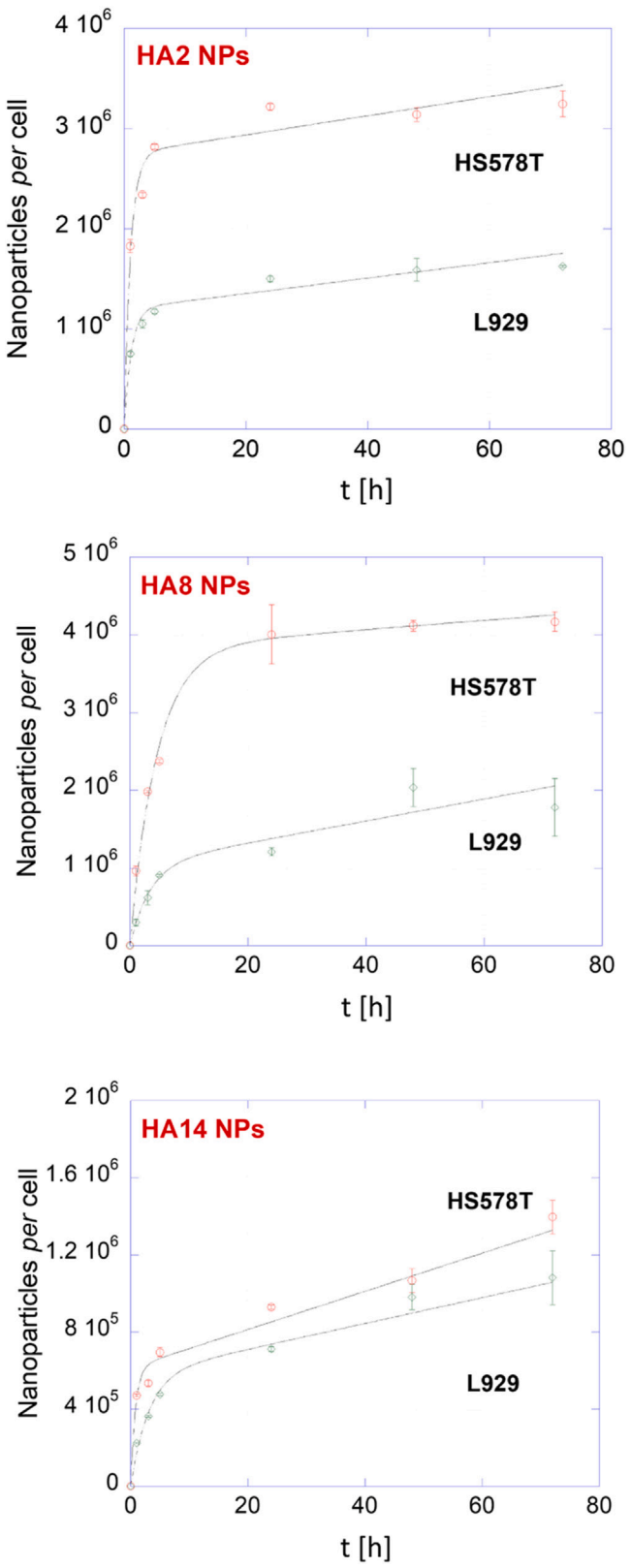

Fig. 6. Uptake kinetics of HA2, HA8 and HA14 NPs by L929 and HS578T cells during continuous exposure, as determined by spectrofluorometric experiments. Solid lines represent the results obtained by data fitting.

Table 3
Model parameters of the kinetics uptake for HA2, HA8 and HA14 NPs against L929 and HS578T cells.

	HA2		HA8		HA14	
	L929	HS578T	L929	HS578T	L929	HS578T
N_{MAX}•10^6	1.77	4.41	1.97	7.17	2.57	2.70
k_B[mg•mL^{-1}•h^{-1}]	0.584	0.595	0.163	0.118	0.0758	0.285
k_D[h^{-1}]	0.267	0.354	0.119	0.0998	0.239	0.934
k_i•10^3 [h^{-1}]	6.39	3.45	13.0	1.54	11.2	15.9

and HA8 NPs were similar, whereas HA14 cell internalization rate decreased. After 24 h, the uptake of HA8 NPs increased considerably, compared to both HA2 and HA14, and a quasi-steady NP internalization was reached for HA2 and HA8 NPs, but not for HA14 NPs. Regarding L929 cells, HA2 and HA14, until 3 h, seem to be internalized in a similar amount, which is higher than the HA8. Differently, after 6 h, HA2 and HA8 reached a similar cell uptake and the HA14 become higher. After 24 h of exposure, HA2 reached the saturation, while HA8 and HA14 after 48 h.

Fig. 6 show the uptake kinetics of HA decorated NPs by L929 and HS578T cells, compared with the results of numerical simulations and Table 3 shows the best-fit parameters used in running the model. The values of N_{MAX}, which expresses the number of NPs that can be internalized by cells after a virtually infinite time, show that the uptake of HA2 and HA8 by HS578T cells is 2.5÷3.6-fold higher than N_{MAX} calculated with L929 cells. In contrast, in the case of HA14, the calculated values of N_{MAX} were similar in both cell populations. Overall, these results suggest an intrinsically higher reactive surface in cancer cells than in healthy cells, with the exception of HA14 NPs, in which the high MW of HA decreases the effectiveness of tumor targeting.

Similarly, the obtained values of the binding and de-binding constants (k_B and k_D) were comparable for HA2 and HA8 formulations in both control and tumor cell lines. On the contrary, in the case of HA14 NPs both constants were approximately 4-fold higher for tumor cells. Furthermore, the internalization constant k_i was found to be higher in the L929 cells for HA2 and HA8 NPs, while being of the same order of magnitude for HA14 against L929 and HS578T cells.

Several mechanisms may occur for the regulation of HA-CD44 binding. One type relates to changes in affinity between HA and a single receptor, exerted by modifications to CD44 glycosylation [14,32,33]. A second type derives from the repetitive structure (GlcNAc1–4GlcUA) contained within the multiple CD44 binding sites (up to a few thousand) of the HA. Individual HA chains can thus interact simultaneously with many CD44 receptors on the cell surface. Moreover, density and arrangement of CD44 receptor on cell surface are changeable, including local enrichment or clustering, and may affect the avidity of a multivalent interaction. A third mechanism may take into account the fact that HA can assume different arrangements on NP surface, due to its flexibility. Thus, the ability to bind several receptors simultaneously, forming real "clusters", depends both on HA chain length and on the number of receptors involved and therefore no longer free to move on the cell membrane. In fact, the distribution of these receptors on cell surface is not uniform, and this implies that different interactions with HA chains derive from the combination between length and flexibility of the exposed HA segment. [35]. Specifically, it is reasonable to assume that long and flexible exposed chain segments can interact with a large number of receptors. This should imply that active targeting efficiency is increasing with increasing HA MW, which seemingly contradicts our findings. Nonetheless, it must be taken into account that the NP production technique used in this work relies upon a blending procedure exploiting the different solubility of different polymers, in the absence of a chemical link. This implies that some random segments of HA chains are actually engaged in the interaction with the hydrophilic poloxamers segments and this interaction, in turn, determines the average length of HA protruding from NPs surface. As a consequence, our results cannot be compared to the case of chemically tethered HA on NP surface [34]. Thanks to preliminary rheological tests, that allowed us to achieve the same viscosity of the aqueous phase used in the NP production, we were able to obtain three different formulations with comparable size, ζ-potential and stability over time. In the context of physically HA decorating NPs, DSC results can provide indications about the spontaneous interaction among PLGA, poloxamers and HA. Actually, the lowest melting heat evolved in the case of HA8 NPs is associated to its favored interaction with the hydrophilic segment of poloxamers. This is further correlated to a promoted HA8 NP internalization and active cell targeting. In the case of HA2 and HA14 formulations, the melting heats are comparable. We speculate that the different active targeting abilities may be dictated by the configuration of HA segments jutting out of NP surface. As for HA2 NPs, the HA segment protruding outwards is long enough to allow a significant, although suboptimal, tumor targeting. Differently, the weak targeting enhancement evoked in the case of HA14 formulation indicates that the length of the superficially exposed HA segments is probably excessive and not fully available for CD44 interaction. Indeed, HA chains of 1400 kDa most probably arrange as large coils, which reduces the possibility to interact with overexpressed receptors on the surface of tumor cells. Overall results indicated that, in the design of NPs, not only HA per se can be a parameter for active targeting but also the conformation assumed on the NPs surface depending on the MW used to decorated NPs.

4. Conclusions

In this work, we have investigated the influence of HA MW (200, 800 and 1437 kDa) used to decorate PLGA-based NPs on their internalization selectivity and kinetics in CD44 overexpressing cells. Considering that NPs have been produced by exploiting the physico-chemical interactions between HA, PLGA and poloxamers, we can infer that HA chain is only partially exposed on NP surface. Moreover, being HA a flexible polymer, it can assume different arrangements on particle surface, thereby influencing CD44 binding.

In this study, we found that 200 kDa HA confers an active targeting toward tumor cells, and this ability increases with increasing HA MW in the case of HA8 NPs, which seemingly possess an optimized interaction with CD44 receptor. Anyhow, most of the targeting ability is lost in the case of HA14 formulation, and this puzzling finding can be reasonably ascribed to an excessive chain length, which favors HA macromolecule self-interactions and, consequently, the formation of random coils on NP surface, which reduces the possibility to interact with overexpressed receptors on the surface of tumor cells.

CRediT authorship contribution statement

Francesca Della Sala: Writing – original draft, Investigation, Writing – review & editing. **Teresa Silvestri**: Investigation Writing – review & editing **Assunta Borzacchiello**: Conceptualization, Supervision, Funding acquisition, Writing – review & editing. **Laura Mayol**: Writing – review & editing, Conceptualization, Supervision. **Luigi Ambrosio**: Resources, Visualization. **Marco Biondi**: Writing – review & editing, Conceptualization, Supervision.

Declaration of Competing Interest

The authors declare that they have no known competing financial interests or personal relationships that could have appeared to influence the work reported in this paper.

Acknowledgments

The authors acknowledge the research project "Advise Drugs and Anti-tumoral Vaccines From The Sea" - Por Campania FESR 2014–2020 AND WITH THE AXIS 1 OO.SS. 1.2.2 / 1.1 CUP B43D18000240007" and the research project "Innovazioni DIagnostiche E Terapeutiche Per Tumori Neuroendocrini, endocrini e per il glioblastoma attraverso una piattaforma tecnologica integrata di competenze cliniche, genomiche, ICT, farmacologiche e farmaceutiche (RARE.PLAT.NET.)" CUP B63D18000380007 - POR CAMPANIA FESR 2014/2020 – ASSE 1 – O.S. 1.2/ CUP.

References

[1] S. Swain, P. Sahu, S. Beg, S. Babu, Nanoparticles for cancer targeting: current and future directions, Curr. Drug Deliv. (2016), https://doi.org/10.2174/1567201813666160713121122.
[2] J. Zhang, H. Tang, Z. Liu, B. Chen, Effects of major parameters of nanoparticles on their physical and chemical properties and recent application of nanodrug delivery system in targeted chemotherapy, Int. J. Nanomed. 12 (2017) 8483–8493, https://doi.org/10.2147/IJN.S148359.
[3] X. Zhen, P. Cheng, K. Pu, Recent advances in cell membrane–camouflaged nanoparticles for cancer phototherapy, Small (2019), https://doi.org/10.1002/smll.201804105.
[4] M. Ferrari, Cancer nanotechnology: opportunities and challenges, Nat. Rev. Cancer. (2005), https://doi.org/10.1038/nrc1566.
[5] R.K. Jain, Transport of molecules, particles, and cells in solid tumors, Annu. Rev. Biomed. Eng. (1999), https://doi.org/10.1146/annurev.bioeng.1.1.241.
[6] S. Tiwari, P. Bahadur, Modified hyaluronic acid based materials for biomedical applications, Int. J. Biol. Macromol. (2019), https://doi.org/10.1016/j.ijbiomac.2018.10.049.
[7] G. Tripodo, A. Trapani, M.L. Torre, G. Giammona, G. Trapani, D. Mandracchia, Hyaluronic acid and its derivatives in drug delivery and imaging: recent advances and challenges, Eur. J. Pharm. Biopharm. (2015), https://doi.org/10.1016/j.ejpb.2015.03.032.
[8] A.I. Caplan, The extracellular matrix is instructive, BioEssays (1986), https://doi.org/10.1002/bies.950050309.
[9] S.C. Owen, S.A. Fisher, R.Y. Tam, C.M. Nimmo, M.S. Shoichet, Hyaluronic acid click hydrogels emulate the extracellular matrix, Langmuir (2013), https://doi.org/10.1021/la305000w.
[10] S.K. Seidlits, Z.Z. Khaing, R.R. Petersen, J.D. Nickels, J.E. Vanscoy, J.B. Shear, C. E. Schmidt, The effects of hyaluronic acid hydrogels with tunable mechanical properties on neural progenitor cell differentiation, Biomaterials (2010), https://doi.org/10.1016/j.biomaterials.2010.01.125.
[11] Y. Zhao, T. Zhang, S. Duan, N.M. Davies, M.L. Forrest, CD44-tropic polymeric nanocarrier for breast cancer targeted rapamycin chemotherapy, Nanomedicine Nanotechnology, Biol. Med. (2014), https://doi.org/10.1016/j.nano.2014.02.015.
[12] Y.-J. Jin, T. Ubonvan, D.-D. Kim, Hyaluronic acid in drug delivery systems, J. Pharm. Investig. (2010), https://doi.org/10.4333/kps.2010.40.s.033.
[13] K.Y. Choi, H. Chung, K.H. Min, H.Y. Yoon, K. Kim, J.H. Park, I.C. Kwon, S.Y. Jeong, Self-assembled hyaluronic acid nanoparticles for active tumor targeting, Biomaterials (2010), https://doi.org/10.1016/j.biomaterials.2009.09.030.
[14] P.M. Wolny, S. Banerji, C. Gounou, A.R. Brisson, A.J. Day, D.G. Jackson, R. P. Richter, Analysis of CD44-hyaluronan interactions in an artificial membrane system: insights into the distinct binding properties of high and low molecular weight hyaluronan, J. Biol. Chem. (2010), https://doi.org/10.1074/jbc.M110.137562.
[15] C.A. De la Motte, V.C. Hascall, J. Drazba, S.K. Bandyopadhyay, S.A. Strong, Mononuclear leukocytes bind to specific hyaluronan structures on colon mucosal smooth muscle cells treated with polyinosinic acid: Polycytidylic acid. Inter-α-trypsin inhibitor is crucial to structure and function, Am. J. Pathol. (2003), https://doi.org/10.1016/S0002-9440(10)63636-X.
[16] T.A. Jokela, A. Lindgren, K. Rilla, E. Maytin, V. Hascall, R. Tammi, M. Tammi, Induction of hyaluronan cables and monocyte adherence in epidermal keratinocytes, Connect. Tissue Res. (2008), https://doi.org/10.1080/03008200802148439.
[17] J. Lesley, I. Gál, D.J. Mahoney, M.R. Cordell, M.S. Rugg, R. Hyman, A.J. Day, K. Mikecz, TSG-6 modulates the interaction between hyaluronan and cell surface CD44, J. Biol. Chem. (2004), https://doi.org/10.1074/jbc.M313319200.
[18] H. Laroui, L. Grossin, M. Léonard, J.F. Stoltz, P. Gillet, P. Netter, E. Dellacherie, Hyaluronate-covered nanoparticles for the therapeutic targeting of cartilage, Biomacromolecules (2007), https://doi.org/10.1021/bm700836y.
[19] N.M. Zaki, A. Nasti, N. Tirelli, Nanocarriers for cytoplasmic delivery: cellular uptake and intracellular fate of chitosan and hyaluronic acid-coated chitosan nanoparticles in a phagocytic cell model, Macromol. Biosci. (2011), https://doi.org/10.1002/mabi.201100156.
[20] V. Belli, D. Guarnieri, M. Biondi, F. della Sala, P.A. Netti, Dynamics of nanoparticle diffusion and uptake in three-dimensional cell cultures, Colloids Surf. B Biointerfaces 149 (2016), https://doi.org/10.1016/j.colsurfb.2016.09.046.
[21] S. Giarra, C. Serri, L. Russo, S. Zeppetelli, G. De Rosa, A. Borzacchiello, M. Biondi, L. Ambrosio, L. Mayol, Spontaneous arrangement of a tumor targeting hyaluronic acid shell on irinotecan loaded PLGA nanoparticles, Carbohydr. Polym. 140 (2016), https://doi.org/10.1016/j.carbpol.2015.12.031.
[22] C. Serri, V. Quagliariello, R.V. Iaffaioli, S. Fusco, G. Botti, L. Mayol, M. Biondi, Combination therapy for the treatment of pancreatic cancer through hyaluronic acid-decorated nanoparticles loaded with quercetin and gemcitabine: a preliminary in vitro study, J. Cell. Physiol. 234 (2019), https://doi.org/10.1002/jcp.27297.
[23] D. Guarnieri, S. Sabella, O. Muscetti, V. Belli, M.A. Malvindi, S. Fusco, E. De Luca, P.P. Pompa, P.A. Netti, Transport across the cell-membrane dictates nanoparticle fate and toxicity: a new paradigm in nanotoxicology, Nanoscale (2014), https://doi.org/10.1039/c4nr02008a.
[24] M. Biondi, S. Fusco, A.L. Lewis, P.A. Netti, Investigation of the mechanisms governing doxorubicin and irinotecan release from drug-eluting beads: mathematical modeling and experimental verification, J. Mater. Sci. Mater. Med. 24 (2013), https://doi.org/10.1007/s10856-013-4992-4.
[25] C. Wilhelm, F. Gazeau, J. Roger, J.N. Pons, J.C. Bacri, Interaction of anionic superparamagnetic nanoparticles with cells: kinetic analyses of membrane adsorption and subsequent internalization, Langmuir (2002), https://doi.org/10.1021/la0257337.
[26] A.L. Doiron, B. Clark, K.D. Rinker, Endothelial nanoparticle binding kinetics are matrix and size dependent, Biotechnol. Bioeng. (2011), https://doi.org/10.1002/bit.23253.
[27] A. Lesniak, A. Salvati, M.J. Santos-Martinez, M.W. Radomski, K.A. Dawson, C. Åberg, Nanoparticle adhesion to the cell membrane and its effect on nanoparticle uptake efficiency, J. Am. Chem. Soc. (2013), https://doi.org/10.1021/ja309812z.
[28] A. Herrera-Gayol, S. Jothy, CD44 modulates HS578T human breast cancer cell adhesion, migration, and invasiveness, Exp. Mol. Pathol. (1999), https://doi.org/10.1006/exmp.1999.2236.
[29] S. Song, H. Qi, J. Xu, P. Guo, F. Chen, F. Li, X. Yang, N. Sheng, Y. Wu, W. Pan, Hyaluronan-based nanocarriers with CD44-overexpressed cancer cell targeting, Pharm. Res. (2014), https://doi.org/10.1007/s11095-014-1393-4.
[30] H.J. Cho, H.Y. Yoon, H. Koo, S.H. Ko, J.S. Shim, J.H. Lee, K. Kim, I. Chan Kwon, D. D. Kim, Self-assembled nanoparticles based on hyaluronic acid-ceramide (HA-CE) and Pluronic ® for tumor-targeted delivery of docetaxel, Biomaterials (2011), https://doi.org/10.1016/j.biomaterials.2011.06.028.
[31] Y. Omori, Q. Li, Y. Nishikawa, T. Yoshioka, M. Yoshida, T. Nishimura, K. Enomoto, Pathological significance of intracytoplasmic connexin proteins: implication in tumor progression, J. Membr. Biol. (2007), https://doi.org/10.1007/s00232-007-9048-6.
[32] S. Garantziotis, R.C. Savani, Hyaluronan biology: a complex balancing act of structure, function, location and context, Matrix Biol. (2019), https://doi.org/10.1016/j.matbio.2019.02.002.
[33] G. Mattheolabakis, L. Milane, A. Singh, M.M. Amiji, Hyaluronic acid targeting of CD44 for cancer therapy: from receptor biology to nanomedicine, J. Drug Target (2015), https://doi.org/10.3109/1061186X.2015.1052072.
[34] S. Mizrahy, S.R. Raz, M. Hasgaard, H. Liu, N. Soffer-Tsur, K. Cohen, R. Dvash, D. Landsman-Milo, M.G.E.G. Bremer, S.M. Moghimi, D. Peer, Hyaluronan-coated nanoparticles: The influence of the molecular weight on CD44-hyaluronan interactions and on the immune response, J. Control. Release (2011), https://doi.org/10.1016/j.jconrel.2011.06.031.
[35] P.M. Wolny, S. Banerji, C. Gounou, A.R. Brisson, A.J. Day, D.G. Jackson, R. P. Richter, Analysis of CD44-hyaluronan interactions in an artificial membrane system: insights into the distinct binding properties of high and low molecular weight hyaluronan, J. Biol. Chem. (2010), https://doi.org/10.1074/jbc.M110.137562.